NANO · MICRO small
www.small-journal.com

Copper Tannic Acid Coordination Nanosheet: A Potent Nanozyme for Scavenging ROS from Cigarette Smoke

*Shichao Lin, Yuan Cheng, He Zhang, Xiaoyu Wang, Yuye Zhang, Yuanjian Zhang, Leiying Miao, Xiaozhi Zhao, and Hui Wei**

The global tobacco epidemic is still a devastating threat to public health. Toxic reactive oxygen species (ROS) in the cigarette smoke cannot be efficiently eliminated by currently available cigarette filters. The resultant oxidative stress causes severe lung injury and further diseases. To tackle this challenge, herein, a novel copper tannic acid coordination (CuTA) nanozyme is reported as a highly active and thermostable ROS scavenger. The CuTA nanozyme exhibits intrinsic superoxide dismutase-like activity, catalase-like activity, and hydroxyl radical elimination capacity. These synergistic antioxidant abilities make the CuTA nanozyme a promising candidate for the improvement of commercial cigarette filters. Mouse model results show that commercial cigarettes loaded with CuTA nanozyme efficiently scavenge ROS in the cigarette smoke, reduce oxidative stress–induced lung inflammation, and minimize the resultant acute lung injury. The developed CuTA nanozyme offers an efficient ROS scavenger with multiple antioxidant ability and opens up new opportunities for the modification of cigarette filters to reduce the toxic effects of cigarette smoke.

1. Introduction

Tobacco use is recognized as a risk factor for most of the eight leading causes of death worldwide.[1–3] Despite the efforts devoted to reducing tobacco use, tobacco epidemic still remains a global health threat.[4] In the smoked cigarettes, toxic reactive oxygen species (ROS) (e.g., oxygen containing radicals and hydrogen peroxide) are generated,[5–7] which cannot be efficiently eliminated by the current cigarette filter techniques.[8] The ROS passed through cigarette filter can induce oxidative stress,[9] cause severe damages to lung tissue and immune system,[6,10] and lead to various diseases (such as lung cancer and chronic obstructive pulmonary disease).[6,11] It is therefore of great significance but challenging to scavenge the generated ROS in cigarette smoke and combat the smoking-induced diseases.

To date, numerous filter modifications have been reported by adding antioxidants or catalytic antioxidants into the cigarette filter. For example, antioxidants extracted from plants including pycnogenol, grape seed extract, and lycopene were loaded into cigarette filters to deplete ROS in cigarette smoke.[12,13] However, their scavenging capacities suffered from their poor thermal stability and limited antioxidant capacity. Recently, catalytic antioxidants were investigated as alternatives to previous antioxidants. Manganese porphyrin derivatives, catalase, and polymer protected

S. C. Lin, Dr. Y. Cheng, X. Y. Wang, Prof. H. Wei
Department of Biomedical Engineering
College of Engineering and Applied Sciences
Nanjing National Laboratory of Microstructures
Jiangsu Key Laboratory of Artificial Functional Materials
Nanjing University
Nanjing, Jiangsu 210093, China
E-mail: weihui@nju.edu.cn

H. Zhang
Department of Periodontology
Nanjing Stomatological Hospital
Medical School of Nanjing University
Nanjing, Jiangsu 210093, China

Y. Y. Zhang, Prof. Y. J. Zhang
Jiangsu Engineering Laboratory of Smart Carbon-Rich Materials and Device
Jiangsu Province Hi-Tech Key Laboratory for Bio-Medical Research
School of Chemistry and Chemical Engineering
Southeast University
Nanjing, Jiangsu 211189, China

The ORCID identification number(s) for the author(s) of this article can be found under https://doi.org/10.1002/smll.201902123.

Prof. L. Y. Miao
Department of Cariology and Endodontics
Nanjing Stomatological Hospital
Medical School of Nanjing University
Nanjing, Jiangsu 210093, China

Dr. X. Z. Zhao
Department of Urology
Drum Tower Hospital
Medical School of Nanjing University
Institute of Urology
Nanjing University
Nanjing, Jiangsu 210008, China

Prof. H. Wei
State Key Laboratory of Analytical Chemistry for Life Science and State Key Laboratory of Coordination Chemistry
School of Chemistry and Chemical Engineering
Nanjing University
Nanjing, Jiangsu 210023, China

DOI: 10.1002/smll.201902123

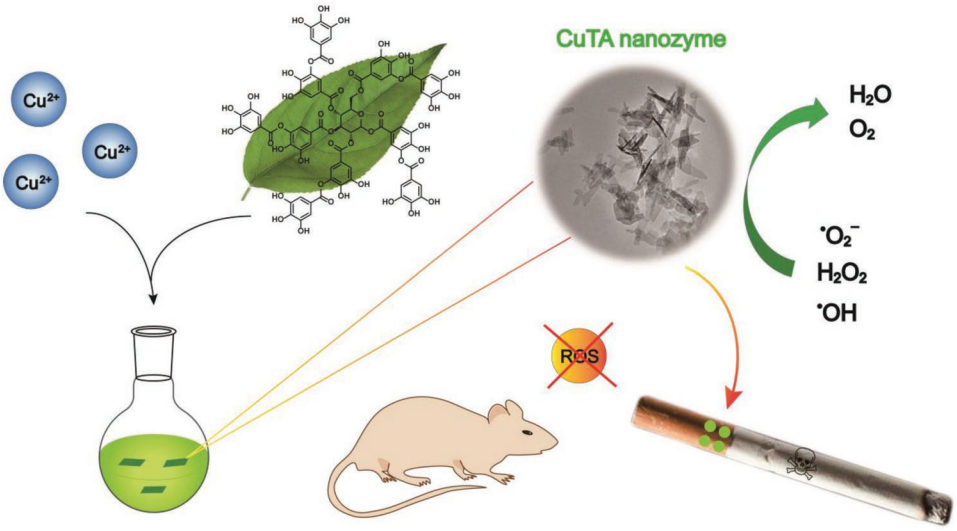

Scheme 1. Schematic illustration of the design and synthesis of ROS scavenging CuTA nanozyme for cigarette filter application.

catalase nanocapsules were explored as new cigarette filter additives.[14–16] Due to much faster reaction rates of catalytic reactions than the uncatalyzed ones, cigarette filters loaded with catalytic antioxidants exhibited greatly improved ROS scavenging efficiency. However, their applications were limited by the poor thermal resistance in hot smoke aerogel. To meet the challenge, highly reactive and thermostable ROS scavengers are urgently demanded.

ROS are also generated in biological organisms and the excessive ROS are harmful.[17] Intracellular enzymes such as superoxide dismutase (SOD), catalase, and glutathione peroxidase have been evolved to scavenge excessive ROS.[18] However, the fragile nature of enzymes imped their practical applications. Recently, nanomaterials with enzyme-like activities (nanozymes) have emerged as promising alternatives to natural enzymes.[19–50] Nanozymes showed higher stability and better tolerance towards harsh environments. Therefore, the exploration of antioxidant enzyme-mimicking nanozymes with high activity and thermal stability offers opportunities to scavenge ROS in cigarette smoke and minimize the smoke-induced damage.

Inspired by antioxidant enzymes, herein, we designed a ROS scavenging antioxidant nanozyme through the coordination of copper and tannic acid (**Scheme 1**). The newly designed copper tannic acid coordination nanosheets (CuTA) nanozyme exhibited SOD-like activity, catalase-like activity, and hydroxyl radical (•OH) eliminating ability. These synergistic ROS scavenging capabilities made CuTA nanozyme as a powerful antioxidant. Moreover, the unique coordination structure endowed the CuTA nanozyme with high thermal stability. The CuTA nanozyme was further loaded into cigarettes to scavenge ROS in the hot smoke aerogel. Animal studies showed that the nanozyme-loaded cigarette filter effectively protected mice from smoking-induced lung destruction and inflammatory disorders.

2. Results and Discussion

As shown in Scheme 1, CuTA nanozyme was synthesized by Cu^{2+}-mediated oxidative coupling assembly of tannic acid. Tannic acid is a ubiquitous natural polyphenol with strong chelating ability.[51,52] As proposed in Figure S1 in the Supporting Information, the self-oxidation of tannic acid was greatly accelerated in the presence of Cu^{2+}.[53,54] The catechol groups of tannic acid were oxidized to highly reactive semi-quinones (*T*′) and quinones (*T*″). Subsequently, *T*′ and *T*″ underwent self-polymerization and coordination to Cu^{2+}. The reaction pH and concentration of Cu^{2+} are two key factors of CuTA morphology evolution. Higher reaction pH promoted the deprotonation of catechol groups and higher concentration of Cu^{2+} ensured the formation of CuTA coordination framework. Therefore, CuTA nanozyme with uniform nanosheet morphology was formed at optimal conditions (i.e., pH = 7.4, 70×10^{-3} M Cu^{2+}) (Figure S2, Supporting Information). Transmission electron microscopy (TEM) image (**Figure 1**a) and scanning electron microscopy (SEM) image (Figure S3, Supporting Information) revealed the ultrathin CuTA nanosheets with an average length and width of 140.5 and 36.9 nm, respectively (Figures S4 and S5, Supporting Information). The structure of CuTA nanozyme was further characterized by X-ray diffraction (XRD). The sharp peaks in Figure 1b indicated a unique crystalline structure of CuTA coordination nanosheets, which was different from other Cu-based materials (i.e., Cu, Cu_2O, CuO, and $Cu(OH)_2$). The coordination between Cu^{2+} and tannic acid was also confirmed by Fourier transform infrared spectra (FTIR) and X-ray photoelectron spectroscopy (XPS). Due to the oxidation of tannic acid and subsequent coordination to Cu^{2+}, the resultant CuTA nanozyme showed splitting and shifting of absorption in the FTIR spectrum when compared with tannic acid itself (Figure 1c). The splitting of absorption centered at 3377 cm^{-1} and shifting of absorption in the fingerprint region indicated the disruption of HO-C vibration of tannic acid after coordinating with Cu^{2+} by the phenolic groups. The content and oxidation state of Cu was revealed by XPS (Figure S6, Supporting Information). The atomic ratio of Cu was 10.86% in the CuTA nanozyme (Table S1, Supporting Information). High resolution spectrum of Cu 2p (Figure 1d) showed the main peaks of Cu 2p3/2 at 935.0 eV and Cu 2p1/2 at 955.2 eV accompanied by their

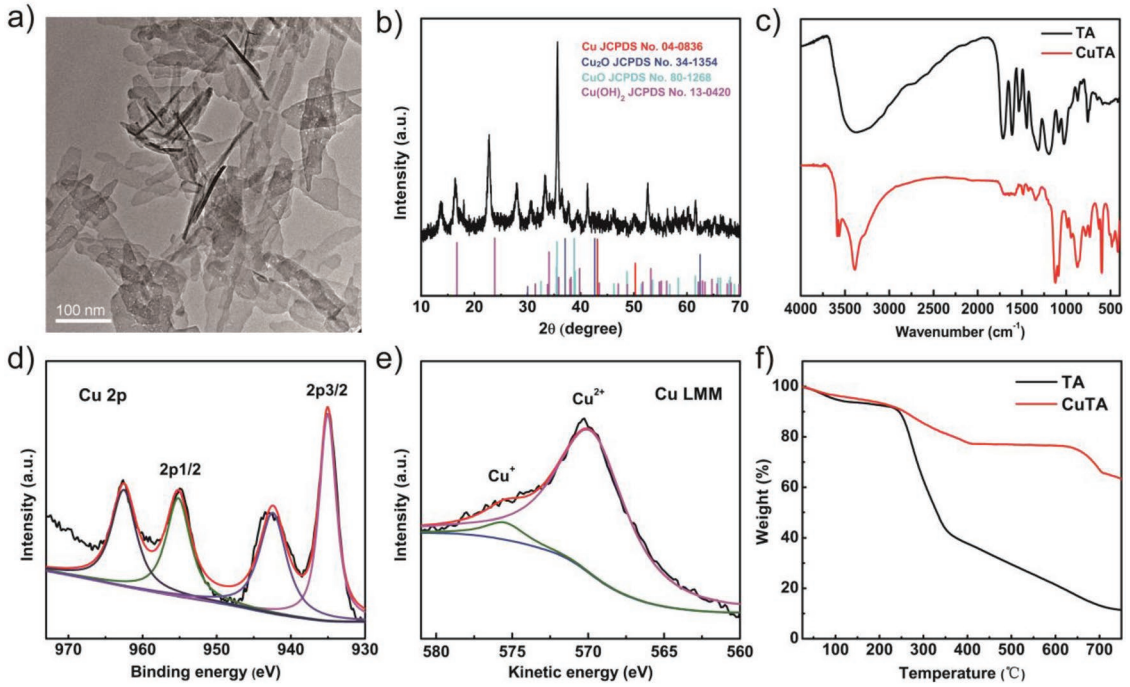

Figure 1. a) Representative TEM image of CuTA nanozyme with nanosheet morphology. b) XRD pattern of CuTA. c) FTIR spectra of TA and CuTA. d) XPS spectra of Cu 2p of CuTA. e) Cu LMM Auger spectra of CuTA. f) Thermogravimetric analysis of TA and CuTA.

characteristic shake-up satellite peaks at 942.5 and 962.5 eV, respectively. X-ray Auger spectra of Cu LMM (Figure 1e) were deconvoluted into the two peaks of Cu^{2+} and Cu^{+}. It revealed that 93.6% of Cu remained in +2 state and no Cu^0 was formed. Interestingly, the coordination of tannic acid to Cu^{2+} greatly enhanced its thermal stability (Figure 1f), which was critical for further cigarette filter applications.

To study the intrinsic SOD-like activity of the CuTA nanozyme, the dismutation of superoxide radicals catalyzed by CuTA nanozyme was probed by iodonitrotetrazolium chloride (INT). INT is a sensitive superoxide indicator, with a strong absorption at the wavelength of 505 nm when reduced by $^{\bullet}O_2^-$. $^{\bullet}O_2^-$ was generated by xanthine and xanthine oxidase in a phosphate buffer (pH 7.4). As shown in **Figure 2**a, in the absence of CuTA nanozyme, INT was reduced by $^{\bullet}O_2^-$, resulting in a prominent absorption peak at 505 nm. However, in the presence of CuTA nanozyme, $^{\bullet}O_2^-$ was decomposed by the SOD-like CuTA nanozyme, inhibiting the reduction of INT by $^{\bullet}O_2^-$. The inhibition of INT reduction as a function of CuTA nanozyme concentration demonstrated the SOD-like activity. $^{\bullet}O_2^-$ elimination level reached over 90% with a CuTA concentration of 1 μg mL^{-1} (Figure 2b), demonstrating the high SOD-like activity of CuTA nanozyme. Then, the catalytic efficiency and thermal stability of SOD-like CuTA nanozyme were compared with natural SOD. CuTA nanozyme with a concentration of 1 μg mL^{-1} exhibited almost the same activity as natural SOD with a concentration of 10 U mL^{-1} (Figure 2c). Moreover, CuTA nanozyme showed high thermal stability in the range of 25 to 80 °C while natural SOD were deactivated at temperatures higher than 40 °C (Figure 2d). pH is also an important factor for the nanozyme activities. We have studied the pH-dependent SOD-like activity of the CuTA nanosheet. As shown in Figure S7 in the Supporting Information, the optimal pH for SOD-mimicking CuTA nanosheet was pH 7.4. CuTA nanosheet remained high SOD-like activity in a broad pH range. We also compared the SOD-like activity of CuTA nanozyme with other representative SOD-mimicking nanozymes (i.e., CeO_2 and Mn_3O_4).[55,56] CuTA nanozyme exhibited higher SOD-like activity at the same conditions (Figure S8, Supporting Information). Together, these results demonstrated that CuTA exhibited excellent SOD-like activity and also high thermal stability for further applications. To understand the high SOD-like activity of CuTA nanozyme, cyclic voltammetry (CV) measurements were carried out to investigate the redox potential of CuTA nanozyme (Figure 2e). Thermodynamically, the dismutation of $^{\bullet}O_2^-$ involved two half reactions (i.e., oxidation and reduction of $^{\bullet}O_2^-$) with the reduction potential E ($O_2/^{\bullet}O_2^-$) = 0.91 V and E ($^{\bullet}O_2^-/H_2O_2$) = –0.18 V.[57] It is expected that the metal centers in an ideal SOD should shuttle between two oxidation states to mediate the two half reactions and the optimal redox potential is about 0.36 V.[58] It is supported by the fact that native SOD enzymes including CuZn-SOD, Mn-SOD, and Ni-SOD have redox potentials close to 0.3 V. The coordination of Cu^{2+} and tannic acid shifted the redox potential of Cu^{2+} from 0.159 to 0.218 V (Figure 2f). The upshift of redox potential of CuTA nanozyme significantly enhanced the shuttling ability of Cu^{2+} active center. Therefore, the high SOD-like activity of CuTA nanozyme was achieved due to the coordination of Cu^{2+} and tannic acid.

The obtained CuTA nanozyme also exhibited intrinsic catalase-like activity and $^{\bullet}OH$ elimination ability. H_2O_2 is another important ROS with high oxidative ability, which is also the downstream product of $^{\bullet}O_2^-$ dismutation. Catalase catalyzes the decomposition of H_2O_2 into H_2O and O_2. The catalase-like activity of CuTA nanozyme was confirmed by the generated O_2

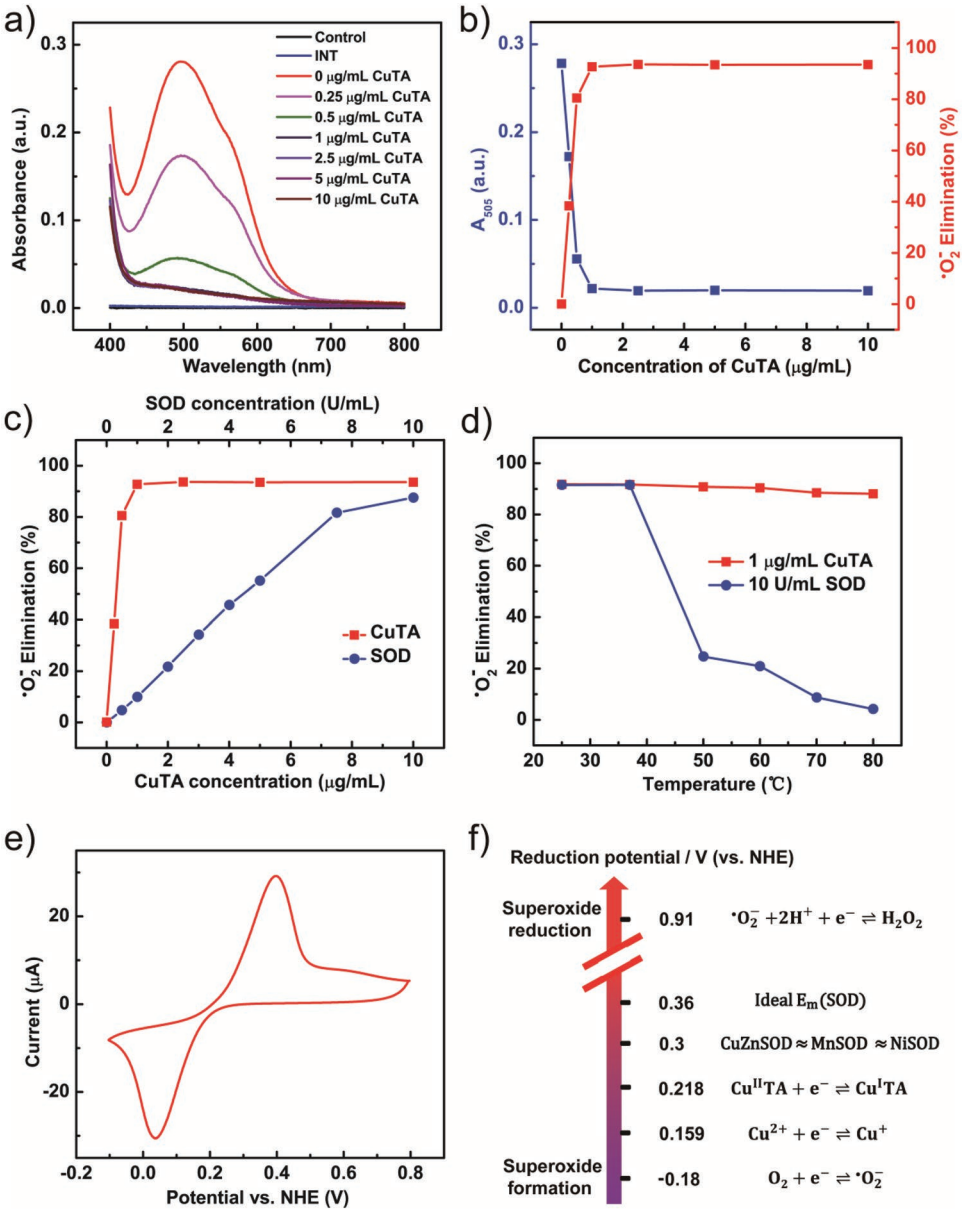

Figure 2. SOD-like activity of CuTA nanozyme. a) Absorption spectra of INT after reaction with $^{\bullet}O_2^-$ in the absence and presence of different concentrations of CuTA nanozyme. b) CuTA nanozyme concentration dependent $^{\bullet}O_2^-$ elimination rates using INT indicator. c) Comparison of concentration dependent $^{\bullet}O_2^-$ elimination rates of CuTA nanozyme and natural SOD. d) $^{\bullet}O_2^-$ elimination rates of CuTA nanozyme and natural SOD after treatments at different temperatures. e) Cyclic voltammogram of CuTA nanozyme. f) Reduction potentials of SOD and CuTA nanozyme involved reactions.

from the decomposition of H_2O_2. As shown in Figure S9 in the Supporting Information, bubbles were generated after adding CuTA nanozyme into the H_2O_2 solution (phosphate buffered, pH 7.4). A dissolved oxygen meter was further used to monitor the generated O_2 dynamically. The decomposition of H_2O_2 into H_2O and O_2 was dependent on the concentration of both substrate and catalyst. The decomposition rates increased with increasing concentration of both H_2O_2 (**Figure 3**a) and CuTA nanozyme (Figure 3b). These results revealed the intrinsic catalase-like activity of CuTA nanozyme. To demonstrate the thermal stability of catalase-mimicking CuTA nanozyme, we studied the catalase-like activity of CuTA nanosheet and the activity of natural catalase after being incubated at different temperature for 1 h. As shown in Figure S10 in the Supporting Information, CuTA nanosheet remained high catalase-like activity even at 80 °C. However, the activity of catalase decreased rapidly with the increase of incubation temperature. The results indicated higher thermal stability of CuTA nanosheet than catalase. Therefore, thermostable CuTA nanosheet is more advantageous than catalase for practical applications. We also investigated the pH-dependent catalase-like activity of CuTA nanozyme. The catalase-like activity of CuTA increased with the increase of pH in the range from pH 5.5 to 10.5 (Figure S11, Supporting Information). This might be ascribed

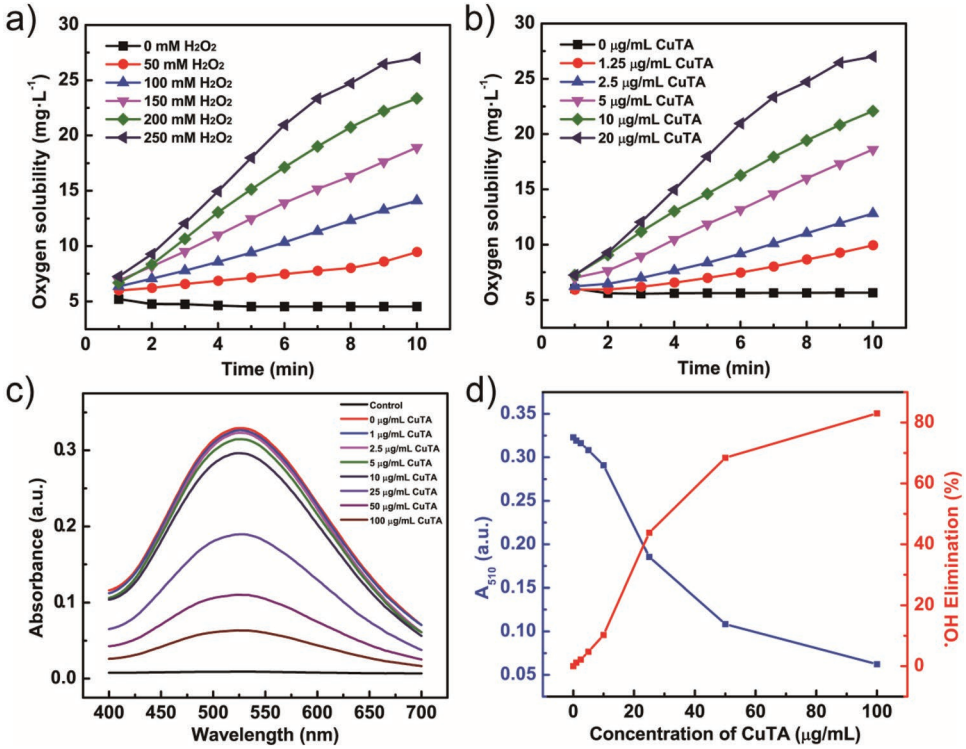

Figure 3. Catalase-like activity and ·OH elimination ability of CuTA nanozyme. a) Increased decomposition rates of H_2O_2 into H_2O and O_2 in the presence of 20 μg mL^{-1} CuTA nanozyme with increased concentration of H_2O_2. b) Increased decomposition rates of 250×10^{-3} M H_2O_2 into H_2O and O_2 with increased concentration of CuTA nanozyme. c) Absorption spectra of SA after reaction with ·OH in the absence and presence of different concentration of CuTA nanozyme. d) CuTA nanozyme concentration dependent ·OH elimination rates using SA indicator.

to the self-decomposition of H_2O_2 at higher pH. Interestingly, CuTA nanozyme also exhibited ·OH elimination ability. ·OH is another highly oxidizing ROS that can cause damages to cell membrane and DNA. The ·OH elimination efficiency of CuTA nanozyme was investigated by salicylic acid (SA), a specific and sensitive ·OH indicator. ·OH was first generated by the classic Fe^{2+}/H_2O_2 Fenton system. SA was attacked by ·OH to form 2,3-dihydroxybenzoic acid with purple color and an absorption peak at 510 nm. CuTA nanozyme could eliminate ·OH and thus less 2,3-dihydroxybenzoic acid was formed. As shown in Figure 3c, the intensity of absorption peak at 510 nm decreased with increasing concentration of CuTA. CuTA nanozyme with a concentration of 100 μg mL^{-1} could eliminate over 80% of ·OH (Figure 3d), demonstrating its high ·OH scavenging capacity. Together, these results revealed that CuTA nanozyme was efficient in scavenging highly oxidizing H_2O_2 and ·OH.

Inspired by the high ROS scavenging activity and thermal stability, CuTA nanozyme was loaded into the cigarette filter to scavenge ROS from the smoke. Highly oxidizing ROS (e.g., $·O_2^-$, H_2O_2, and ·OH) in the smoke are toxic and cannot be efficiently eliminated by the current cigarette filter techniques. The ROS scavenging efficiency of CuTA nanozyme loaded cigarette filter was evaluated by exposing generated smoke to probing solutions containing different ROS indicators. The generated $·O_2^-$ in smoked cigarette was detected by INT. As shown in **Figure 4**a, INT was reduced by $·O_2^-$ in the cigarette smoke generated without CuTA nanozyme, resulting in the prominent absorption at 505 nm. However, the absorption was greatly inhibited for the cigarette with CuTA nanozyme, revealing a $·O_2^-$ scavenging efficiency of 87.0% (Figure 4d). A 10-acetyl-3,7-dihydroxyphenoxazine (ADHP)-horseradish peroxidase (HRP) system was used to detect H_2O_2. HRP catalyzes the oxidation of ADHP in the presence of H_2O_2 to produce a fluorescent signal. As shown in Figure 4b, ADHP was oxidized by H_2O_2 in the cigarette smoke without CuTA nanozyme, resulting in the fluorescence peak at 585 nm. The fluorescence was suppressed for the cigarette with CuTA nanozyme, indicating a H_2O_2 scavenging efficiency of 68.9% (Figure 4d). To detect ·OH, 1,4-phthalic acid (PTA) was introduced as a fluorogenic indicator. PTA reacts with ·OH to produce fluorescent 2-hydroxyterephthalic acid. As shown in Figure 4c, PTA captured ·OH in the cigarette smoke without CuTA nanozyme, resulting in the fluorescent signal with a peak at 405 nm. The fluorescence was reduced for the cigarette with CuTA nanozyme, indicating a ·OH scavenging efficiency of 34.6% (Figure 4d). To further confirm the synergistic ROS scavenging ability, 2′,7′-dichlorodihydrofluorescein (DCFH), a general ROS indicator, was introduced to evaluate the total ROS in the smoke. As shown in Figure 4e, DCFH reacted with ROS in the cigarette smoke without CuTA nanozyme, giving prominent fluorescence with a peak at 525 nm. The fluorescence was greatly inhibited for the cigarette with CuTA nanozyme, indicating a total ROS scavenging efficiency of 71.7% (Figure 4f). To confirm the critical role of CuTA rather than TA in scavenging ROS from smoke, we have loaded the same amount of TA as CuTA in the filter and evaluated the ROS scavenging capacity. As shown

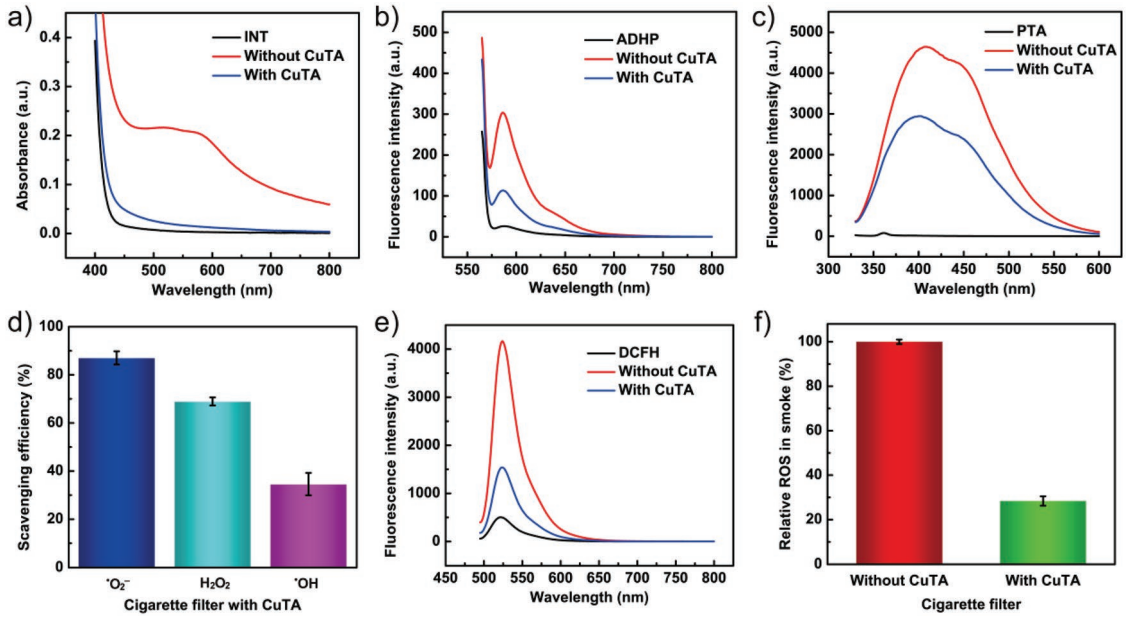

Figure 4. Effective scavenging of ROS from cigarette smoke by CuTA nanozyme loaded cigarette filter. a) Absorption spectra of INT, the superoxide indicator, b) fluorescence spectra of ADHP, the HRP assisted hydrogen peroxide probe, and c) fluorescence spectra of PTA, the hydroxyl radical probe, after exposure to cigarette smoke passing through cigarette filter without or with CuTA nanozyme loaded. d) Superoxide, hydrogen peroxide, and hydroxyl radical scavenging efficiency of cigarette filter with CuTA nanozyme loaded. e) Fluorescence spectra of DCFH, a general ROS indicator, after exposure to cigarette smoke passing through cigarette filter without or with CuTA nanozyme loaded. f) Reduction of ROS in cigarette smoke by CuTA nanozyme loaded cigarette filter, as indicated by DCFH.

in Figure S12 in the Supporting Information, TA loaded filter only reduced 17.6%, 16.9%, and 35.6% of $^{\bullet}O_2^-$, H_2O_2, and $^{\bullet}OH$, respectively. We further used DCFH, a general ROS probe to evaluate the total ROS scavenging efficiency of filter with TA loaded. As shown in Figure S13 in the Supporting Information, only 21.6% of ROS was scavenged for filter with TA loaded, indicating the critical role of CuTA in scavenging ROS. Together, these results demonstrated that CuTA nanozyme loaded cigarette filter exhibited high efficiency in scavenging ROS from smoked cigarette.

Due to the high performance of scavenging ROS from hot smoke aerogel, the CuTA nanozyme was further applied in cigarette filter modification to minimize the cigarette smoke induced destruction in a mouse model. We first evaluated the potential Cu toxicity induced by CuTA. We collected the cigarette smoke after passing through cigarette filters and evaluated the Cu contents by inductive coupled plasma atomic emission spectrometry (ICP-AES). As shown in Table S2 in the Supporting Information, no significant difference of Cu contents was observed between the groups of filter without CuTA and with CuTA, indicating no additional Cu was released from CuTA. Therefore, cigarette filter with CuTA loaded would not pose additional risk of Cu exposure as compared with normal cigarette filter. As shown in **Figure 5**a, mice were placed in a glass container equipped with a homemade air extractor. Cigarette smoke passed through the commercial filter with (or without) CuTA nanozyme and channeled into the container. Mice were exposed to the resultant smoke in three consecutive days. As indicated by the hematoxylin and eosin (H&E) staining of lung tissues, mice exposed to smoke from commercial cigarettes without CuTA loaded in the filter suffered from severe lung damage (Figure 5c). Increased thickness of bronchi capillary walls was observed with signs of neutrophil and lymphocyte infiltration, indicating the acute lung destruction. However, lung tissues of mice exposed to smoke from commercial cigarettes with CuTA loaded exhibited significantly less pathological alterations (Figure 5d) when compared with normal lung tissues in the control group (Figure 5b). ROS in the cigarette smoke were toxic and could not be efficiently eliminated by the commercial cigarette filter. Therefore, the generated ROS induced oxidative stress in the lung tissues of mice, causing acute lung injury. Encouragingly, CuTA nanozyme in the filter could effectively scavenge ROS in the passing cigarette smoke, protecting the mice from ROS-induced destruction. The pro-inflammatory cytokine evaluation also confirmed the protecting role of ROS scavenging CuTA nanozyme. As shown in Figure 5e,f, mice exposed to smoke from commercial cigarettes without CuTA loaded in the filter exhibited elevated level of pro-inflammatory cytokines including TNF-α and IL-1β. However, mice of the group with CuTA loaded in the filter suffered significantly less pulmonary inflammation with normal level of TNF-α and IL-1β in the lung tissues. These results demonstrated that CuTA nanozyme could efficiently scavenge ROS in the cigarette smoke, minimize ROS-induced oxidative stress in lung tissues, and protect the mice from smoke-induced acute lung injury.

3. Conclusions

In conclusion, we have designed and synthesized a ROS scavenging CuTA nanozyme by the coordination of Cu^{2+} and tannic acid. The obtained CuTA nanozyme exhibited intrinsic SOD-like

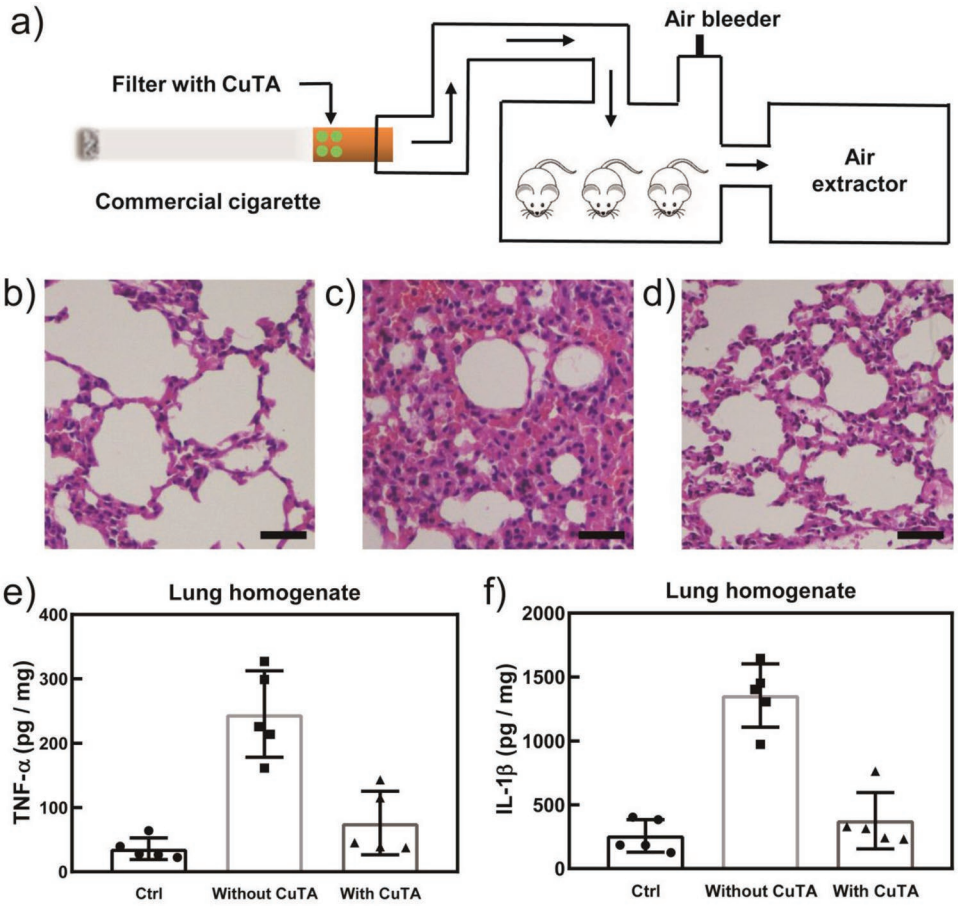

Figure 5. Cigarette filter application of ROS scavenging CuTA nanozyme to minimize the cigarette smoke induced destruction in a mouse model. a) Scheme of the setup to expose mice to cigarette smoke for the animal model study. H&E staining of lung tissues of mice b) without cigarette smoke treatment, c) exposed to cigarette smoke passing through cigarette filter without CuTA nanozyme loaded, and d) exposed to cigarette smoke passing through cigarette filter with CuTA nanozyme loaded. Scale bars in (b–d) 50 μm. Concentrations of e) TNF-α and f) IL-1β pro-inflammatory cytokines in the lung tissues of mice.

activity, catalase-like activity, and •OH elimination capacity. These characteristics made CuTA nanozyme a highly efficient antioxidant system to scavenge ROS. The developed CuTA nanozyme was further applied in cigarette filter modification. CuTA nanozyme loaded commercial cigarette filter efficiently scavenged ROS in the cigarette smoke, protecting mice exposed to cigarette smoke from pulmonary inflammation and acute lung injury. The developed CuTA nanozyme offers an excellent ROS scavenger with multiple antioxidant capacity and paves a new avenue to the modification of cigarette filters for reducing toxic effects of cigarette smoke

4. Experimental Section

Chemicals: Tannic acid, cupric sulfate pentahydrate ($CuSO_4{\cdot}5H_2O$), ferrous sulfate ($FeSO_4$), and sodium hydroxide (NaOH) were purchased from Sinopharm Chemical Reagent Co., Ltd. Hydrogen peroxide (H_2O_2, 30%) and SA were obtained from Aladdin Chemical Reagent Co., Ltd. INT was purchased from J&K Scientific Ltd. Xanthine and xanthine oxidase were supplied by Sigma-Aldrich. SOD from porcine erythrocytes was obtained from Shanghai Yuanye Biological Technology Co., Ltd. Other chemicals were of at least analytical reagent grade. All chemical regents were used as received without any further purification. All aqueous solutions were prepared with deionized water (18.2 MΩ cm, Millipore).

Instrumentation: SEM was performed on a Zeiss Ultra 55 microscope (Zeiss, Germany). TEM images were collected on a Tecnai F20 microscope (FEI, USA) at an acceleration voltage of 200 kV. Powder XRD data were obtained at room temperature on a Rigaku Ultima diffractometer (Rigaku, Japan) by using Cu Kα radiation. XPS spectra were collected by a PHI 5000 VersaProbe XPS microscope (UlVAC-PHI, Japan). UV–vis absorption spectra were recorded on a UV–vis spectrophotometer (Cary-100, Agilent Technologies, USA). Fluorescence spectra were measured on a Hitachi F-4600 spectrometer (Hitachi Co. Ltd., Japan). Fourier transform infrared spectra were performed on NEXUS-870 (NICOLET, USA). Thermogravimetric analysis was carried out on a NETZSCH STA 409 PC/PG (NETZSCH, Germany) with a heating rate of 10 °C min^{-1}.

Synthesis of CuTA Nanozyme: CuTA nanozyme were prepared through an oxidative coupling assembly strategy. In a typical synthesis, 27 mg of tannic acid and 875 mg $CuSO_4{\cdot}5H_2O$ were dissolved in 50 mL deionized water to make a homogeneous solution. After adjusting its pH to 7.4 by 2 M NaOH, the solution was heated to 50 °C and kept for 3 h. The product was separated by centrifugation and washed thoroughly with deionized water. The purified light green product was dried at 60 °C under vacuum overnight for further experiments.

SOD-Like Activity of CuTA Nanozyme: The SOD-like activity of CuTA nanozyme was evaluated by monitoring the amount of $^{\bullet}O_2^-$ scavenged with the INT probe. First, $^{\bullet}O_2^-$ was generated by mixing xanthine (0.6×10^{-3} M) and xanthine oxidase (0.05 U mL^{-1}) in phosphate buffer (0.1 M, pH 7.4) at 37 °C. After 10 min, CuTA nanozyme was added into

the solution and kept for 30 min at 37 °C. Finally, the remained $^{\bullet}O_2^-$ was detected by INT probe. INT was reduced by $^{\bullet}O_2^-$ to a red product with an absorption peak at 505 nm, which was further quantified by UV–vis absorption spectroscopy. The scavenging percentage of $^{\bullet}O_2^-$ was calculated by the following equation: elimination (%) = $[(A_1 - A_2)/(A_1 - A_0)] \times 100\%$, where A_0 was the absorbance of INT and A_1 and A_2 were the absorbance of reduced INT at 505 nm in the absence and presence of CuTA nanozyme, respectively.

Electrochemical Measurements: CV measurements were performed on an electrochemical analyzer (CHI 660E, CHI Instrument). CuTA nanozyme film sprayed on a glassy carbon electrode (GCE) served as the working electrode. An Ag/AgCl (KCl-saturated) and a platinum wire were used as the reference electrode and the counter electrode, respectively. CV experiments were carried out after purging the HEPES buffer solution (0.1 M, pH 7.4) with nitrogen for 30 min at room temperature. The scan rate was 10 mV s^{-1}. Normal hydrogen electrode (NHE) potential was calculated by the equation: E (NHE) = E (Ag/AgCl) + 0.197 V.

Catalase-Like Activity of CuTA Nanozyme: The catalase-like activity of CuTA nanozyme was studied at room temperature by measuring the generated oxygen using a dissolved oxygen meter (JPSJ-605, Leici, China). Briefly, CuTA nanozyme and H_2O_2 were successively added into 3.0 mL phosphate buffer solution (0.1 M, pH 7.4). The generated oxygen solubility (unit: mg L^{-1}) was monitored in 10 min. The catalase-like activity of CuTA nanozyme was directly revealed by the catalyzed decomposition of H_2O_2 into H_2O and O_2.

Hydroxyl Radical Scavenging Activity of CuTA Nanozyme: The $^{\bullet}OH$ was generated through Fenton reaction of 0.2×10^{-3} M H_2O_2 and 0.2×10^{-3} M $FeSO_4$ for 3 min. Then, CuTA nanozyme was added into the solution and incubated for another 3 min to eliminate $^{\bullet}OH$. Finally, 1×10^{-3} M SA was introduced to detect remained $^{\bullet}OH$. SA was oxidized by $^{\bullet}OH$ to 2, 3-dihydroxybenzoic acid with purple color and an absorption peak at 510 nm. The remained $^{\bullet}OH$ was quantified by UV–vis absorption spectroscopy. The scavenging percentage of $^{\bullet}OH$ was calculated by the following equation: elimination (%) = $[(A_1 - A_2)/(A_1 - A_0)] \times 100\%$, where A_0 was the absorbance of SA and A_1 and A_2 were the absorbance of 2, 3-dihydroxybenzoic acid at 510 nm in the absence and presence of CuTA nanozyme, respectively.

Cigarette Filter Application: All the research cigarettes were Hongmei cigarettes from Hongta Tobacco Group, China. CuTA nanozyme was loaded into the cigarette filter with a dose of 50 mg per cigarette. To fabricate the CuTA nanozyme loaded cigarettes, one quarter of cellulose acetate fiber near tobacco in each cigarette filter was replaced with 50 mg of CuTA nanozyme powder.

For in vitro ROS scavenging evaluation, ROS probe containing solutions were exposed to smoke generated by one cigarette without or with CuTA nanozyme loaded in the filter. INT (0.5×10^{-3} M in phosphate buffer, pH 7.4) was used to detect $^{\bullet}O_2^-$. The scavenging efficiency of $^{\bullet}O_2^-$ was calculated by the following equation: scavenging efficiency (%) = $[(A_1 - A_2)/(A_1 - A_0)] \times 100\%$, where A_0 was the absorbance of INT and A_1 and A_2 were the absorbance of reduced INT at 505 nm for the cigarette without and with CuTA nanozyme loaded in the filter, respectively. An ADHP-HRP system (0.1×10^{-3} M ADHP and 0.4 U mL^{-1} HRP in pH 4.5 NaOAc buffer, excitation wavelength of 560 nm) was used to detect H_2O_2. The scavenging efficiency of H_2O_2 was calculated by the following equation: scavenging efficiency (%) = $[(F_1 - F_2)/(F_1 - F_0)] \times 100\%$, where F_0 was the fluorescence intensity of ADHP in the presence of HRP and F_1 and F_2 were the fluorescence intensity of oxidized ADHP at 585 nm for the cigarette without and with CuTA nanozyme loaded in the filter, respectively. PTA (0.2×10^{-3} M in pH 7.4 phosphate buffer, excitation wavelength of 320 nm) was used to detect $^{\bullet}OH$. The scavenging efficiency of $^{\bullet}OH$ was calculated by the following equation: scavenging efficiency (%) = $[(F_1 - F_2)/(F_1 - F_0)] \times 100\%$, where F_0 was the fluorescence intensity of PTA and F_1 and F_2 were the fluorescence intensity of 2-hydroxyterephthalic acid at 405 nm for the cigarette without and with CuTA nanozyme loaded in the filter, respectively. The total ROS was detected by DCFH (0.02×10^{-3} M in pH 7.4 phosphate buffer, excitation wavelength of 485 nm). The relative ROS percentage in smoke was calculated by the following equation: relative ROS in smoke (%) = $[(F_1 - F_2)/(F_1 - F_0)] \times 100\%$, where F_0 was the fluorescence intensity of DCFH and F_1 and F_2 were the fluorescence intensity of oxidized DCFH at 525 nm for the cigarette without and with CuTA nanozyme loaded in the filter, respectively.

For animal model studies, ICR male mice (6 weeks) were randomly divided into three groups with five mice per group ($n = 5$). Mice in Group 1 served as control and were not treated with cigarette smoke. Groups 2 and 3 were experimental groups using commercial cigarettes without or with CuTA loaded in the filter to generate smoke, respectively. Each of the two experimental groups was placed in a glass container equipped with a homemade air extractor. After passing through the cigarette filter, cigarette smoke was channeled into the glass container by the air extractor induced negative pressure. Mice in the glass container were exposed to the smoke generated by four cigarettes each day for 3 days. The flow rate of generated smoke was controlled at 0.2 L min^{-1}. Mice were taken out from the container for 15 min to breathe fresh air after every exposure of smoke generated by half of one cigarette. At the 4th day, all the mice were sacrificed to collect the lung tissues for histopathological and pro-inflammatory cytokines evaluation. For histopathological evaluation, the middle lope of right lung of each group was collected and rinsed with normal saline and fixed with 10% formalin. The fixed lung tissues were then embedded in paraffin, sectioned at a thickness of 4 mm, and stained with H&E. Pathological changes were examined under optical microscope. For pro-inflammatory cytokines evaluation, the amount of TNF-α and IL-1β in lung homogenate was quantified by ELISA test. The lower lope of the left lung of each mouse was weighted and homogenated in 3 mL saline at 4 °C. The resultant homogenate was centrifuged at 2000 rpm for 20 min at 4 °C, and the supernatant was collected for evaluation. Commercial mouse IL-1β and TNF-α ELISA Kit (Neobioscience, China) was utilized for the determination of pro-inflammatory cytokines including IL-1β and TNF-α in lung homogenate. All animal experimental protocols were approved by the Institutional Animal Care and Use Committee, Drum Tower Hospital, Medical School of Nanjing University. The animal studies were also overseen by Jiangsu Association for Laboratory Animal Science, with an accreditation number of 220170161.

Supporting Information

Supporting Information is available from the Wiley Online Library or from the author.

Acknowledgements

S.C.L., Y.C., and H.Z. contributed equally to this work. This work was supported by National Natural Science Foundation of China (21722503, 21874067, and 91859112), Natural Science Foundation of Jiangsu Province (BK20180340), 973 Program (2015CB659400), PAPD Program, Shuangchuang Program of Jiangsu Province, Open Funds of the State Key Laboratory of Analytical Chemistry for Life Science (SKLACLS1704), Open Funds of the State Key Laboratory of Coordination Chemistry (SKLCC1819), and Fundamental Research Funds for the Central Universities (21314380145).

Conflict of Interest

The authors declare no conflict of interest.

Keywords

acute lung injury, cigarette smoke, copper tannic acid coordination, oxidative stress, ROS scavenging nanozymes

Received: April 27, 2019
Revised: July 27, 2019
Published online:

[1] WHO Report on the Global Tobacco Epidemic, 2008: The MPOWER package, World Health Organization, Geneva **2008**.
[2] J. Britton, *Lancet* **2015**, *385*, 924.
[3] H. Wipfli, J. M. Samet, *Annu. Rev. Public Health* **2016**, *37*, 149.
[4] WHO Report on the Global Tobacco Epidemic, 2017: Monitoring Tobacco Use and Prevention Policies; Executive Summary, World Health Organization, Geneva **2017**.
[5] A. L. Bluhm, J. Weinstein, J. A. Sousa, *Nature* **1971**, *229*, 500.
[6] S. Onizawa, K. Aoshiba, M. Kajita, Y. Miyamoto, A. Nagai, *Pulm. Pharmacol. Ther.* **2009**, *22*, 340.
[7] W. A. Pryor, K. Stone, *Ann. N. Y. Acad. Sci.* **1993**, *686*, 12.
[8] K. Korschelt, R. Ragg, C. S. Metzger, M. Kluenker, M. Oster, B. Barton, M. Panthofer, D. Strand, U. Kolb, M. Mondeshki, S. Strand, J. Brieger, M. Nawaz Tahir, W. Tremel, *Nanoscale* **2017**, *9*, 3952.
[9] H. van der Vaart, D. S. Postma, W. Timens, N. H. ten Hacken, *Thorax* **2004**, *59*, 713.
[10] M. R. Stämpfli, G. P. Anderson, *Nat. Rev. Immunol.* **2009**, *9*, 377.
[11] S. S. Hecht, *Nat. Rev. Cancer* **2003**, *3*, 733.
[12] X. Shen, K. Zhong, X. Sun, H. Lu, Y. Shen, L.-X. Yu, *Anal. Lett.* **2010**, *43*, 446.
[13] D. Zhang, Y. Tao, J. Gao, C. Zhang, S. Wan, Y. Chen, X. Huang, X. Sun, S. Duan, F. Schönlau, P. Rohdewald, B. Zhao, *Toxicol. Ind. Health* **2002**, *18*, 215.
[14] L. Liu, W. Yu, D. Luo, Z. Xue, X. Qin, X. Sun, J. Zhao, J. Wang, T. Wang, *Adv. Funct. Mater.* **2015**, *25*, 5159.
[15] X. Lu, Z. Hua, G. Du, X. Ma, J. Cao, Z. Yang, J. Chen, *Free Radical Res.* **2008**, *42*, 244.
[16] K. R. Smith, D. L. Uyeminami, U. P. Kodavanti, J. D. Crapo, L.-Y. Chang, K. E. Pinkerton, *Free Radicals Biol. Med.* **2002**, *33*, 1106.
[17] C. C. Winterbourn, *Nat. Chem. Biol.* **2008**, *4*, 278.
[18] C. Michiels, M. Raes, O. Toussaint, J. Remacle, *Free Radicals Biol. Med.* **1994**, *17*, 235.
[19] Y. Huang, J. Ren, X. Qu, *Chem. Rev.* **2019**, *119*, 4357.
[20] F. Wang, E. Ju, Y. Guan, J. Ren, X. Qu, *Small* **2017**, *13*, 1603051.
[21] H. Wang, C. Liu, Z. Liu, J. Ren, X. Qu, *Small* **2018**, *14*, 1703710.
[22] J. Wu, X. Wang, Q. Wang, Z. Lou, S. Li, Y. Zhu, L. Qin, H. Wei, *Chem. Soc. Rev.* **2019**, *48*, 1004.
[23] H. Zhang, X. Liang, L. Han, F. Li, *Small* **2018**, *14*, 1803256.
[24] Z. Zhang, B. Liu, J. Liu, *Small* **2017**, *13*, 1602730.
[25] H. Wei, E. Wang, *Chem. Soc. Rev.* **2013**, *42*, 6060.
[26] N. A. Kotov, *Science* **2010**, *330*, 188.
[27] L. Z. Gao, J. Zhuang, L. Nie, J. B. Zhang, Y. Zhang, N. Gu, T. H. Wang, J. Feng, D. L. Yang, S. Perrett, X. Y. Yan, *Nat. Nanotechnol.* **2007**, *2*, 577.
[28] Z. Xu, Z. Qiu, Q. Liu, Y. Huang, D. Li, X. Shen, K. Fan, J. Xi, Y. Gu, Y. Tang, J. Jiang, J. Xu, J. He, X. Gao, Y. Liu, H. Koo, X. Yan, L. Gao, *Nat. Commun.* **2018**, *9*, 3713.
[29] G. Y. Tonga, Y. D. Jeong, B. Duncan, T. Mizuhara, R. Mout, R. Das, S. T. Kim, Y. C. Yeh, B. Yan, S. Hou, V. M. Rotello, *Nat. Chem.* **2015**, *7*, 597.
[30] A. Gupta, R. Das, G. Yesilbag Tonga, T. Mizuhara, V. M. Rotello, *ACS Nano* **2018**, *12*, 89.
[31] Z. Zhang, X. Zhang, B. Liu, J. Liu, *J. Am. Chem. Soc.* **2017**, *139*, 5412.
[32] B. Liu, Z. Sun, P.-J. J. Huang, J. Liu, *J. Am. Chem. Soc.* **2015**, *137*, 1290.
[33] J. P. Chen, S. Patil, S. Seal, J. F. McGinnis, *Nat. Nanotechnol.* **2006**, *1*, 142.
[34] R. W. Tarnuzzer, J. Colon, S. Patil, S. Seal, *Nano Lett.* **2005**, *5*, 2573.
[35] C. Hao, A. Qu, L. Xu, M. Sun, H. Zhang, C. Xu, H. Kuang, *J. Am. Chem. Soc.* **2019**, *141*, 1091.
[36] S. S. Ali, J. I. Hardt, K. L. Quick, J. S. Kim-Han, B. F. Erlanger, T. T. Huang, C. J. Epstein, L. L. Dugan, *Free Radicals Biol. Med.* **2004**, *37*, 1191.
[37] L. L. Dugan, L. L. Tian, K. L. Quick, J. I. Hardt, M. Karimi, C. Brown, S. Loftin, H. Flores, S. M. Moerlein, J. Polich, S. D. Tabbal, J. W. Mink, J. S. Perlmutter, *Ann. Neurol.* **2014**, *76*, 393.
[38] Y. Huang, Z. Liu, C. Liu, E. Ju, Y. Zhang, J. Ren, X. Qu, *Angew. Chem.* **2016**, *128*, 6758.
[39] W. Zhang, S. Hu, J. J. Yin, W. He, W. Lu, M. Ma, N. Gu, Y. Zhang, *J. Am. Chem. Soc.* **2016**, *138*, 5860.
[40] Y. Zhang, Z. Y. Wang, X. J. Li, L. Wang, M. Yin, L. H. Wang, N. Chen, C. H. Fan, H. Y. Song, *Adv. Mater.* **2016**, *28*, 1387.
[41] W. Y. Zhen, Y. Liu, L. Lin, J. Bai, X. D. Jia, H. Y. Tian, X. Jiang, *Angew. Chem., Int. Ed.* **2018**, *57*, 10309.
[42] H. J. Kwon, D. Kim, K. Seo, Y. G. kIm, S. I. Han, T. Kang, M. Soh, T. Hyeon, *Angew. Chem., Int. Ed.* **2018**, *57*, 9408.
[43] Q. Q. Bao, P. Hu, Y. Y. Xu, T. S. Cheng, C. Y. Wei, L. M. Pan, J. L. Shi, *ACS Nano* **2018**, *12*, 6794.
[44] F. Li, T. Y. Li, C. X. Sun, J. H. Xia, Y. Jiao, H. P. Xu, *Angew. Chem., Int. Ed.* **2017**, *56*, 9910.
[45] Y. L. Liu, K. L. Ai, X. Y. Ji, D. Askhatova, R. Du, L. H. Lu, J. J. Shi, *J. Am. Chem. Soc.* **2017**, *139*, 856.
[46] N. Singh, M. A. Savanur, S. Srivastava, P. D'Silva, G. Mugesh, *Angew. Chem., Int. Ed.* **2017**, *56*, 14267.
[47] M. Soh, D. W. Kang, H. G. Jeong, D. Kim, D. Y. Kim, W. Yang, C. Song, S. Baik, I. Y. Choi, S. K. Ki, H. J. Kwon, T. Kim, C. K. Kim, S. H. Lee, T. Hyeon, *Angew. Chem., Int. Ed.* **2017**, *56*, 11399.
[48] Y. Hu, H. Cheng, X. Zhao, J. Wu, F. Muhammad, S. Lin, J. He, L. Zhou, C. Zhang, Y. Deng, P. Wang, Z. Zhou, S. Nie, H. Wei, *ACS Nano* **2017**, *11*, 5558.
[49] X. Wang, X. J. Gao, L. Qin, C. Wang, L. Song, Y.-N. Zhou, G. Zhu, W. Cao, S. Lin, L. Zhou, K. Wang, H. Zhang, Z. Jin, P. Wang, X. Gao, H. Wei, *Nat. Commun.* **2019**, *10*, 704.
[50] Z. Chen, Z. Wang, J. Ren, X. Qu, *Acc. Chem. Res.* **2018**, *51*, 789.
[51] J. Guo, Y. Ping, H. Ejima, K. Alt, M. Meissner, J. J. Richardson, Y. Yan, K. Peter, D. von Elverfeldt, C. E. Hagemeyer, F. Caruso, *Angew. Chem., Int. Ed.* **2014**, *53*, 5546.
[52] T. S. Sileika, D. G. Barrett, R. Zhang, K. H. Lau, P. B. Messersmith, *Angew. Chem., Int. Ed.* **2013**, *52*, 10766.
[53] Z. Chen, C. Wang, J. Chen, X. Li, *J. Am. Chem. Soc.* **2013**, *135*, 4179.
[54] M. Mochizuki, S.-i. Yamazaki, K. Kano, T. Ikeda, *Biochim. Biophys. Acta, Gen. Subj.* **2002**, *1569*, 35.
[55] F. Muhammad, A. Wang, W. Qi, S. Zhang, G. Zhu, *ACS Appl. Mater. Interfaces* **2014**, *6*, 19424.
[56] J. Yao, Y. Cheng, M. Zhou, S. Zhao, S. Lin, X. Wang, J. Wu, S. Li, H. Wei, *Chem. Sci.* **2018**, *9*, 2927.
[57] Y. Sheng, I. A. Abreu, D. E. Cabelli, M. J. Maroney, A. F. Miller, M. Teixeira, J. S. Valentine, *Chem. Rev.* **2014**, *114*, 3854.
[58] L. Bixenmann, J. He, M. Liang, W. Tremel, *Prog. Biochem. Biophys.* **2018**, *45*, 148.